(Electronic Supplementary Information)

Effective solar light-driven isothiazolinone degradation by morphology and oxygen vacancy modified Gd-doped BiOCl

Lei Xu[a], Zhiren Guo[a], Xiao Zhang[a], Menglin Zhang[a], Jinying Li[a], Dongxiang Zhang[a,b,*], Xiyan Xu[a,*]

a School of Chemistry and Chemical Engineering, Beijing Institute of Technology, Beijing 102488, PR China

b Department of Chemistry, MSU-BIT University, Shenzhen, 517182, PR China

**Corresponding authors:*

Dr. Xiyan Xu, E-mail: xiyanxu@bit.edu.cn

Dr. Dongxiang Zhang, E-mail: boris@bit.edu.cn

The electronic supplementary information includes 13 pages, 1 text, 2 tables, and 16 figures.

Text S1:

Characterization of materials

The scanning electron microscopy (SEM) was performed by ZEISS Supra 55 SAPPHIRE (Germany) equipped with energy-dispersive X-ray analysis (EDS, Oxford Instruments X-Max). High-resolution transmission electron microscopy (HRTEM) was performed by Talos F200X (USA) with an acceleration voltage of 200 kV.

The X-ray diffraction (XRD, Cu Kα = 0.154 nm, Voltage = 40 kV, electric current = 150 mA) was measured by Rigaku Ultima IV (Japan) to investigate the crystallographic information of synthesized BiOCl-based photocatalysts. The scanning setting was: the rate equal of $5°\cdot min^{-1}$ and the 2θ range of 10-80°. The Jade 6.0 was further performed to analyze and identify corresponding data.

X-ray photoelectron spectroscopy (XPS) was measured by PHI 5000 VersaProbe III (Japan) with monochromatic Al Kα irradiation to study the valence state and composition of photocatalyst surface elements.

TriStar II 3020 (USA) was measured to analyze the porous structure of BiOCl-based photocatalysts. According to the tests of N_2 adsorption-desorption, the Brunauer-Emmett-Teller (BET) method was performed to calculate the specific surface area (S_{BET}) of BiOCl-based photocatalysts. The total pore volume (V_{Total}) and the average pore size distribution (D_{Ave}) were assessed in terms of the adsorption amount at a P/P_0 of 0.99 and the Barrett–Joyner–Halenda (BJH) formula, respectively.

The Fourier transform infrared (FT-IR) was performed by Thermo IS5 (USA) to analyze the chemical structure of obtained photocatalysts. UV–vis diffuse reflectance spectra (DRS) were measured by TU-1901 (CHINA) and $BaSO_4$ was used as the

reference background. Raman spectra were measured by Horiba scientific-LabRAM HR evolution (Japan) with an excitation laser wavelength of 532 nm. The photoluminescence (PL) spectra with wavelength region of 400 nm-600 nm, were measured by F-7000 FL (Japan). And the excitation wavelength was set to 235 nm.

Electron paramagnetic resonance (EPR) was performed by Bruker A300 (Germany) to identify the production of Ovs and free radicals. As for the identifications of free radicals, 5,5-dimethyl-1-pyrroline N-oxide (DMPO) was adopted as trapping agent. The solvent used for testing $^{\bullet}OH$ was water and for $O_2^{\bullet-}$ was methanol. For each test, 10 mg sample was scattered in the 10 ml solvent in a quartz capillary (1 mm × 100 mm), and 200 μL sample solution and 10 mM trapping agent were well mixed.

Electrochemical impedance spectroscopy (EIS), Transient photocurrent responses, and Mott-Schottky (M-S) tests were measured by the CS310H electrochemical workstation (China) with a three-electrode system. The three-electrode system consists of counter electrode (Pt plate), reference electrode (Ag/AgCl), and working electrode (ITO). 1 mM $K_3Fe(CN)_6$, 1 mM $K_4Fe(CN)_6$, and 0.1 mM KCl after deoxidation were used as the electrochemical impedance spectroscopy (EIS) test electrolyte. The electrolyte of photocurrent and Mott-Schottky(M-S) test was 0.1M Na_2SO_4 solution. A 300 W Xe lamp was performed as the Transient photocurrent experiments light source. For each test, 6 mg of photocatalyst was dispersed in 10 μL Nafion and 3mL ethanol mixed solution by ultrasound and then 100 μL suspension was coated on the ITO conductive glass.

Table S1. The spectrum parameters of the fitted XPS peaks.

PGE-BiOCl				BiOCl			
Peak	Center	Area	FWHM	Peak	Center	Area	FWHM
Bi $4f_{7/2}$	158.6	61299.1	1.5	Bi $4f_{7/2}$	159.3	211209.4	2.0
Bi $4f_{5/2}$	163.9	45974.3	1.5	Bi $4f_{5/2}$	164.6	162905.1	2.1
Bi $4f_{7/2}$	159.5	23920.7	2.3	Cl $2p_{3/2}$	197.6	9622.8	1.2
Bi $4f_{5/2}$	164.7	17871.5	2.1	Cl $2p_{1/2}$	199.1	16254.3	2.1
Cl $2p_{3/2}$	197.1	3994.3	1.4	O 1s	529.7	8255.7	1.3
Cl $2p_{1/2}$	198.6	5137.0	2.1	O 1s	531.9	28684.9	3.4
O 1s	529.3	4855.8	1.5				
O 1s	532.0	37274.7	2.9				
O 1s	533.8	6018.4	2.1				
N 1s	399.9	4006.0	2.4				

Table S2. The corresponding parameters of carrier lifetime of the obtained BiOCl-based materials from TR-PL tests.

Catalysts	τ_1 (ns)	A_1 (%)	τ_2 (ns)	A_2 (%)	Ave.τ (ns)
BiOCl	0.88	73.07	3.78	26.93	2.66
E-BiOCl	1.08	76.99	4.16	23.01	2.73
GE-BiOCl	1.34	72.99	5.02	27.01	3.48
PGE-BiOCl	2.25	79.37	7.59	20.63	4.74

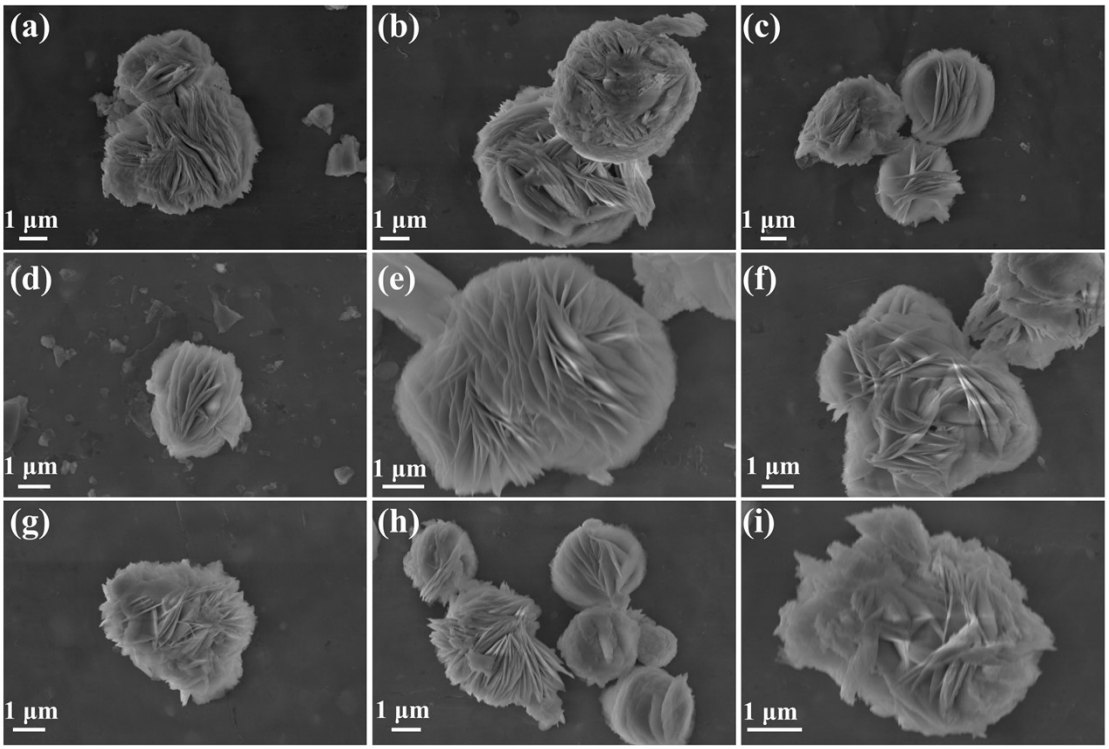

Figure S1. SEM images of PGE-BiOCl with different PVP addition: (a) 0.2 g; (b) 0.4 g; (c) 0.6 g; (d) 0.8 g; (e) 1.0 g; (f) 1.2 g; (g) 1.4 g; (h) 1.6 g; (i) 1.8 g.

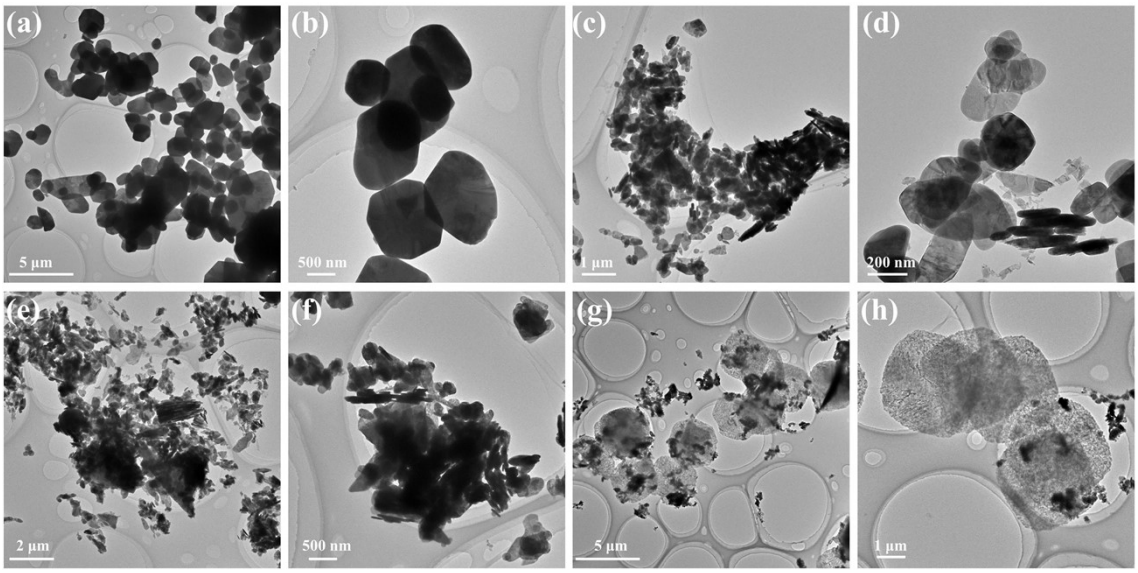

Figure S2. TEM images of BiOCl-based catalysts: (a-b) BiOCl; (c-d) E-BiOCl; (e-f) GE-BiOCl; (g-h) PGE-BiOCl.

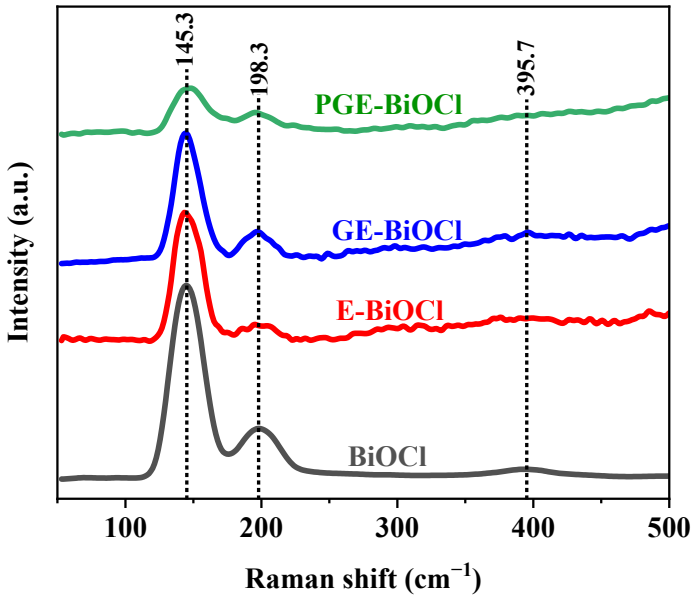

Figure S3. Raman spectra of BiOCl-based catalysts.

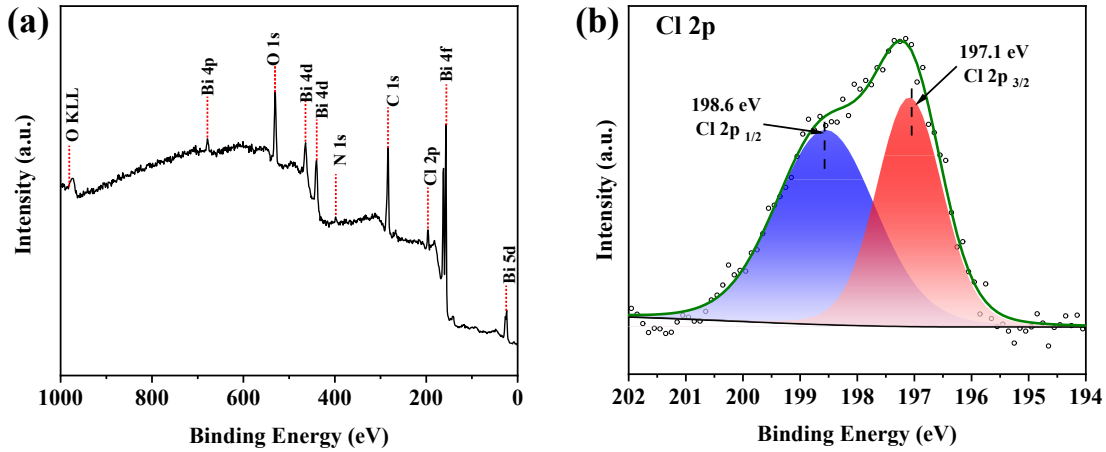

Figure S4. (a) The relative full XPS spectrum of PGE-BiOCl; (b) the Cl 2p spectrum of PGE-BiOCl.

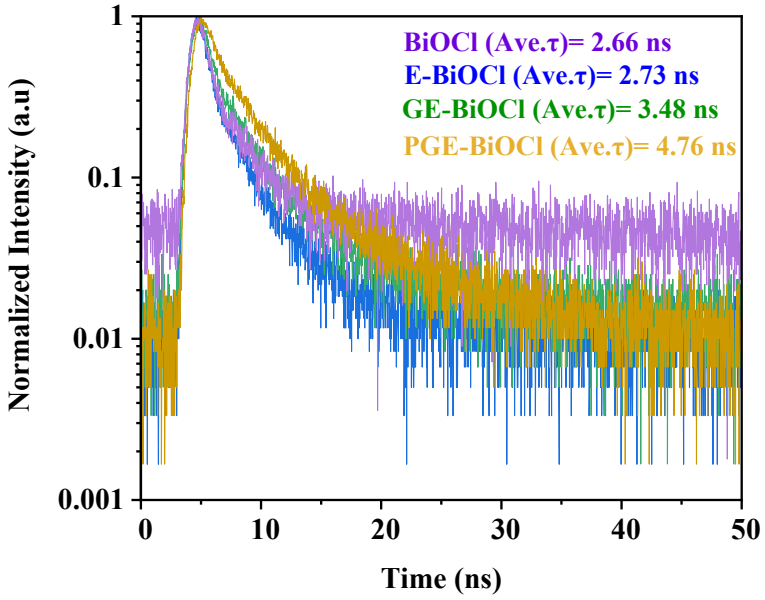

Figure S5. TR-PL decay of BiOCl-based materials.

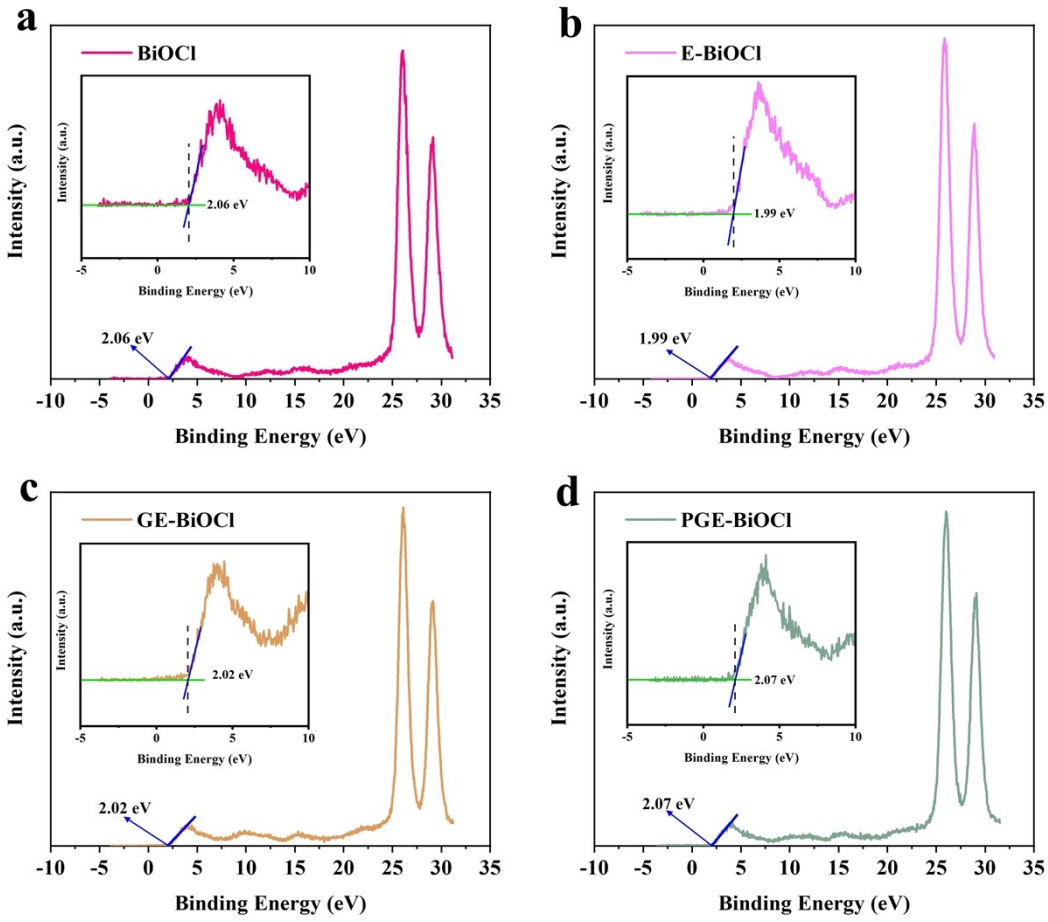

Figure S6. Valence band XPS spectra of the BiOCl-based catalysts.

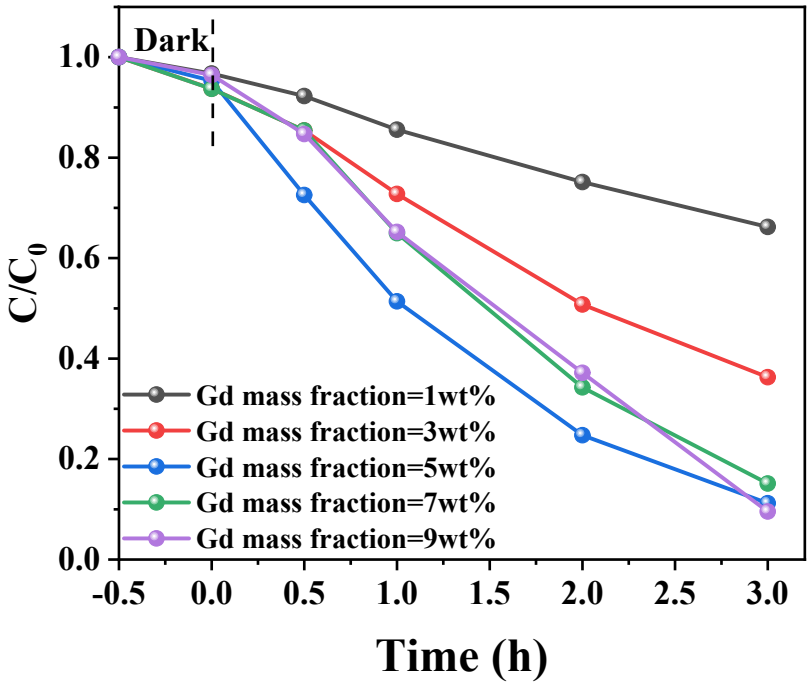

Figure S7. Degradation toward BIT by PGE-BiOCl under different Gd mass ratios.

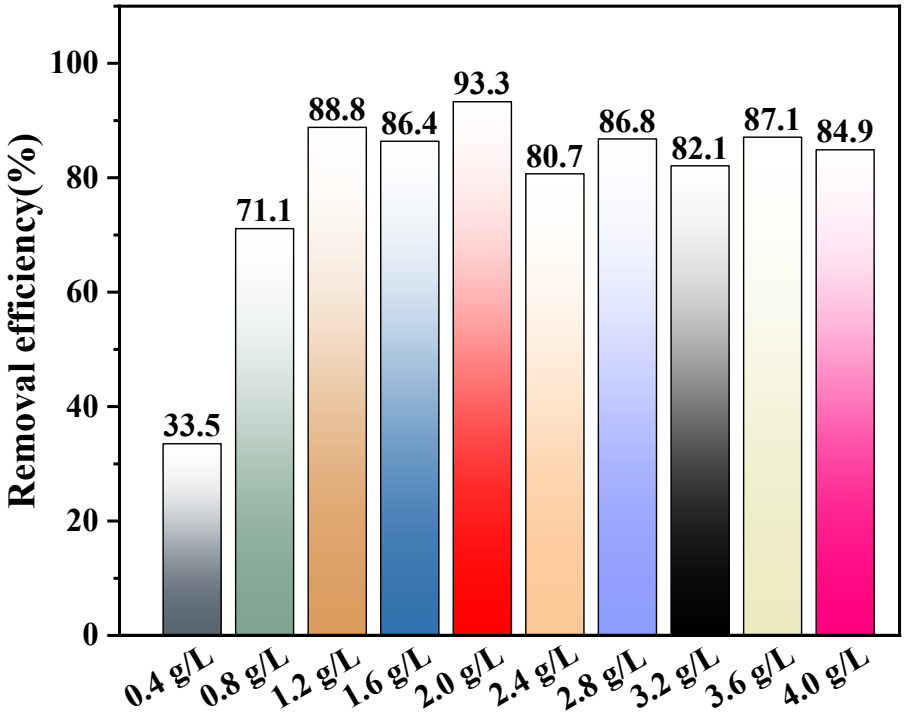

Figure S8. Photocatalytic activity of PGE-BiOCl catalysts with different dosages toward BIT removal under visible light.

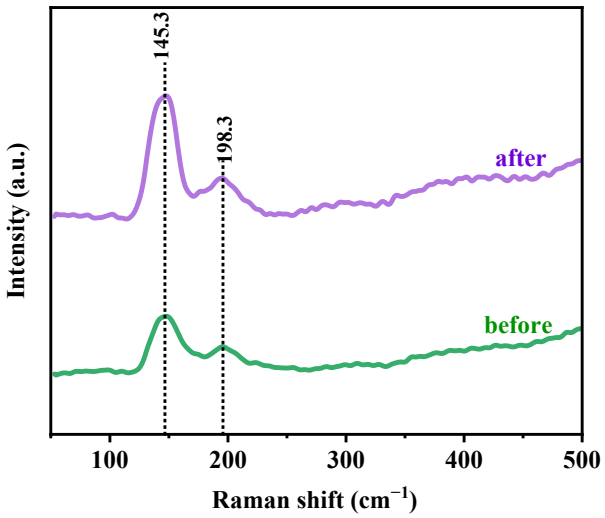

Figure S9. Raman spectra of PGE-BiOCl before and after use.

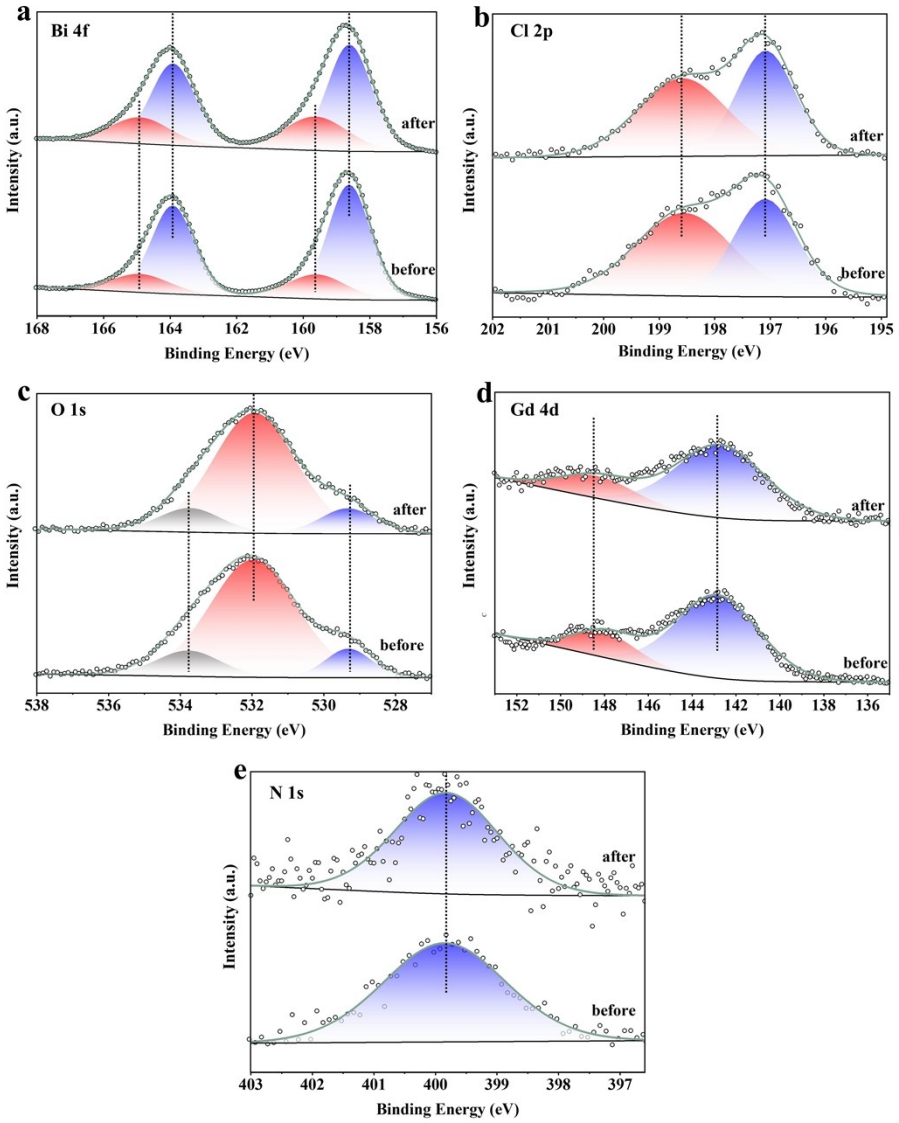

Figure S10. XPS spectra of (a) Bi 4f; (b) Cl 2p; (c) O 1s; (d) Gd 4d; (e) N 1s of PGE-

BiOCl before and after use.

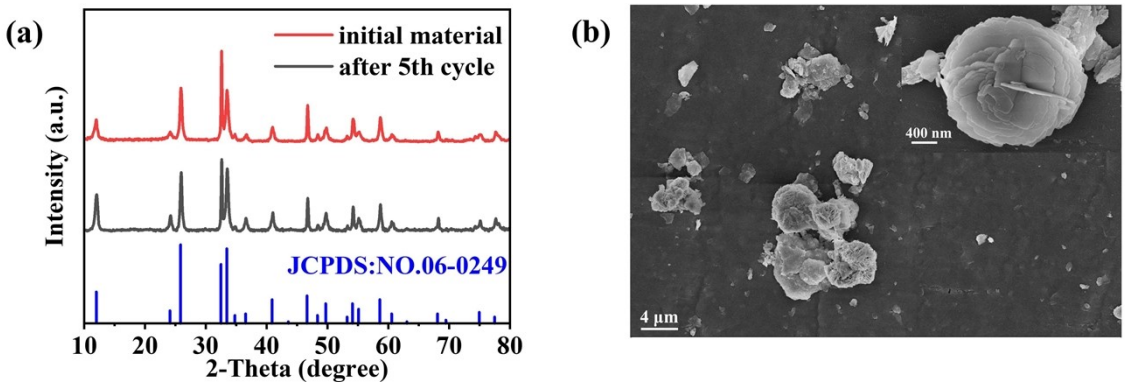

Figure S11. (a) XRD patterns of PGE-BiOCl before and after use; (b) SEM images of PGE-BiOCl after use.

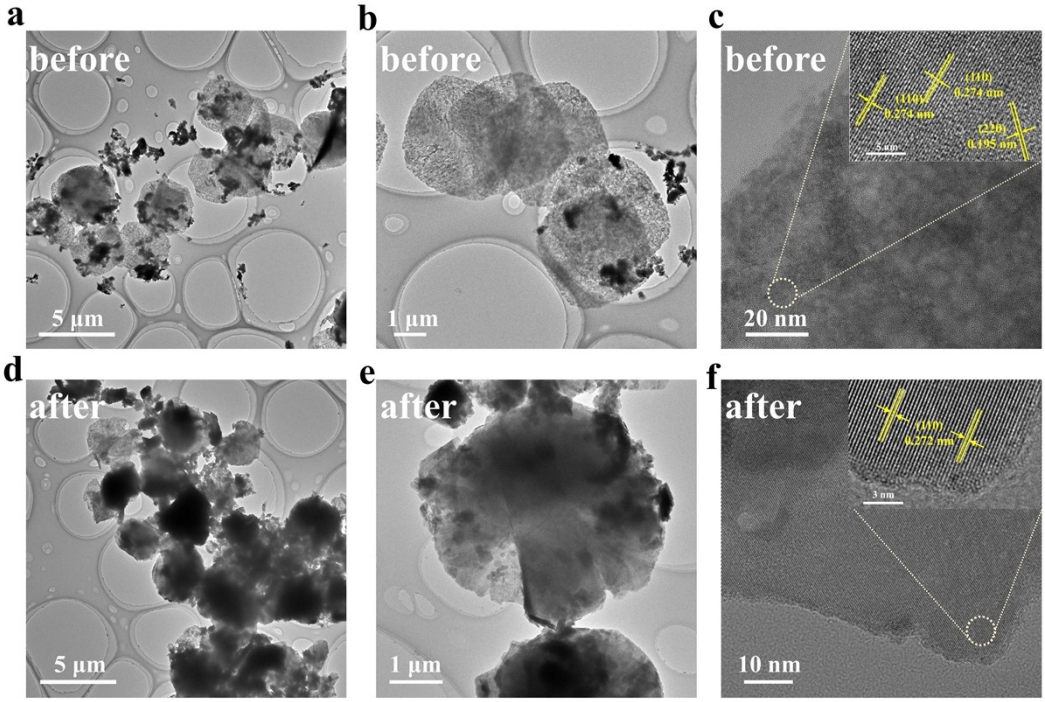

Figure S12. TEM images of PGE-BiOCl before and after use.

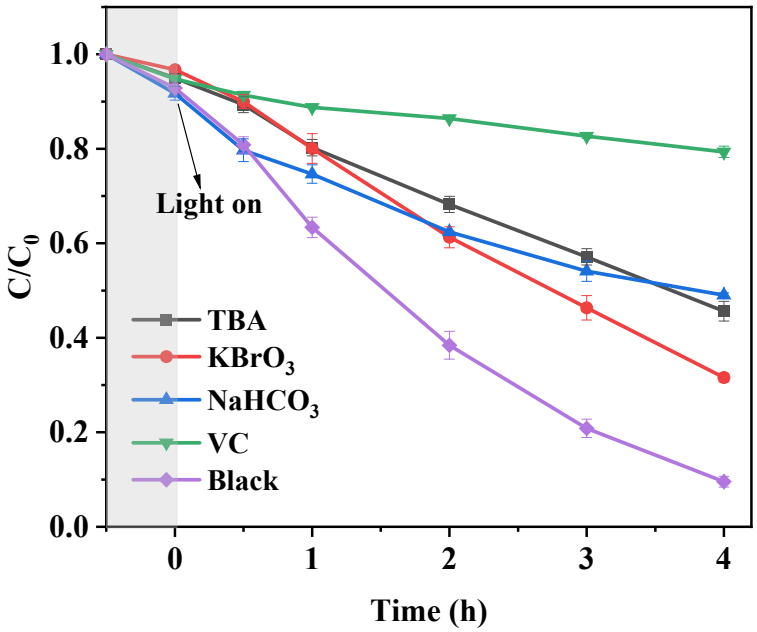

Figure S13. Effects of different scavengers on the photocatalytic degradation toward BIT.

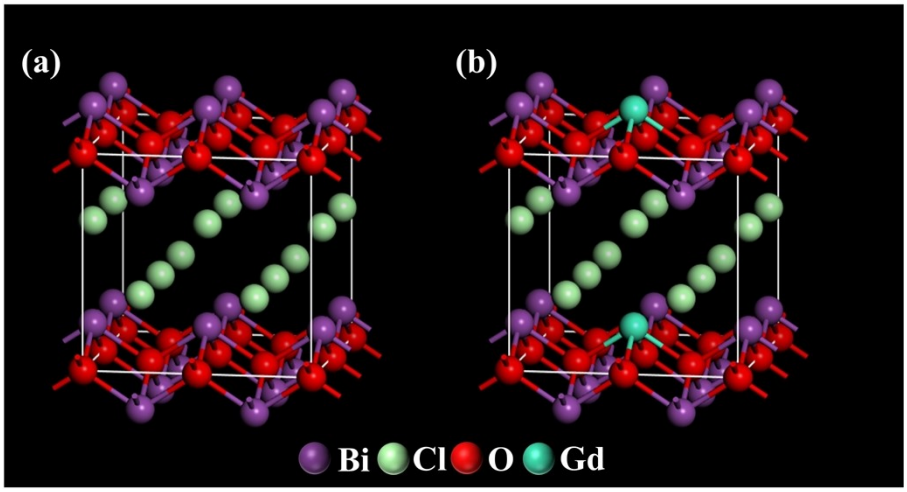

Figure S14. Constructed micro-structures of the (a) BiOCl; (b) PGE-BiOCl.

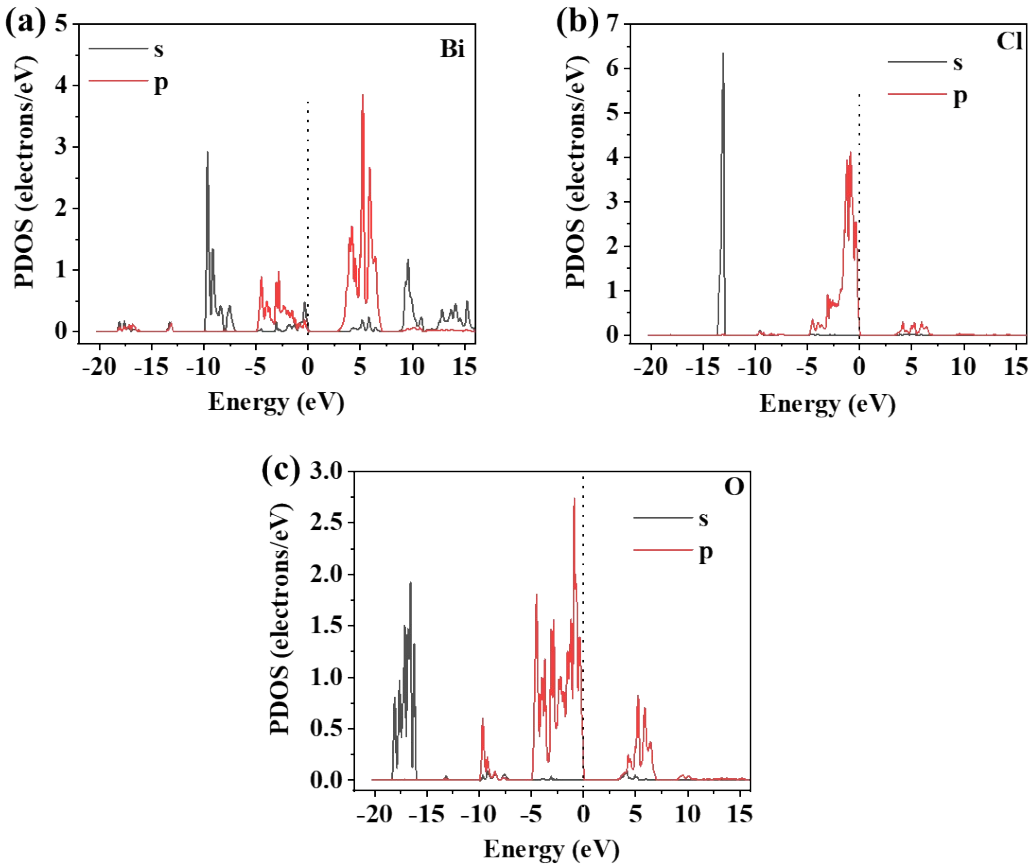

Figure S15. The Projected Density of States (PDOS) of (a) Bi; (b) Cl; (c) O of BiOCl.

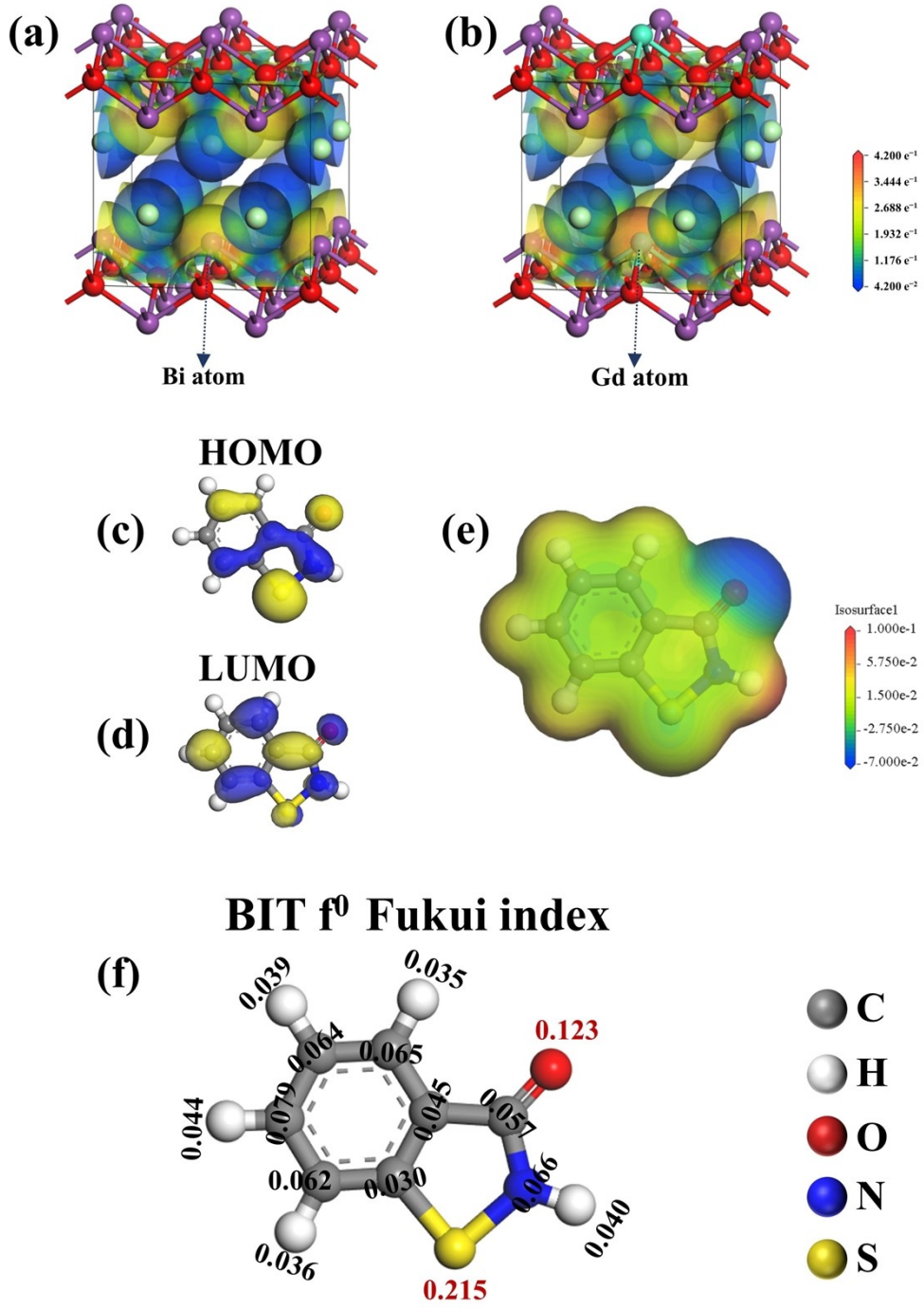

Figure S16. The ESP distribution of (a) BiOCl; (b) PGE-BiOCl; the (c) HOMO; (d) LUMO of BIT; (e) the ESP distribution of BIT; (f) the f^0 Fukui index of BIT.